Geophysical Research Letters

RESEARCH LETTER
10.1029/2019GL084534

Wildfire Impact on Environmental Thermodynamics and Severe Convective Storms

Yuwei Zhang[1,2], Jiwen Fan[1], Timothy Logan[3], Zhanqing Li[2], and Cameron R. Homeyer[4]

[1]Atmospheric Sciences and Global Change Division, Pacific Northwest National Laboratory, Richland, WA, USA, [2]Department of Atmospheric and Oceanic Science, University of Maryland, College Park, MD, USA, [3]Department of Atmospheric Sciences, Texas A&M University, College Station, TX, USA, [4]School of Meteorology, University of Oklahoma, Norman, OK, USA

Key Points:
- A new model capability to computationally efficiently account for the impact of heat flux on thermodynamics from wildfires in WRF-Chem is developed
- Both the heat and aerosol emissions from wildfires invigorate the pyroconvection, enlarge hail size, and enhance lightning
- Effects of heat from wildfire on convective intensity, hail size, and lightning are more significant than those of aerosol emissions

Supporting Information:
- Supporting Information S1

Correspondence to:
J. Fan,
jiwen.fan@pnnl.gov

Citation:
Zhang, Y., Fan, J., Logan, T., Li, Z., & Homeyer, C. R. (2019). Wildfire impact on environmental thermodynamics and severe convective storms. *Geophysical Research Letters*, *46*, 10,082–10,093. https://doi.org/10.1029/2019GL084534

Received 16 APR 2019
Accepted 9 AUG 2019
Accepted article online 15 AUG 2019
Published online 21 AUG 2019

Abstract Wildfires are extreme events associated with weather, climate, and environment and have been increasing globally in frequency, burn season length, and burned area. It is of great interest to understand the impacts of wildfires on severe convective storms through releasing heat and aerosols into the atmosphere. We have developed a model capability that can account for the impact of sensible heat fluxes from wildfires on thermodynamics and is computationally efficient. The pyrocumulonimbus clouds associated with the Texas Mallard Fire on 11–12 May 2018 are well simulated by accounting for both heat and aerosols emitted from the wildfire. Both heat and aerosol effects increase low-level temperatures and midlevel buoyancy and enhance convective intensity. Intensified convection along with more supercooled liquid condensate due to stronger vertical transport results in larger hailstones and enhanced lightning. The effects of heat flux on the convective extremes are more significant than those of aerosol emissions.

Plain Language Summary The length of wildfire burning season and burned area have been increasing globally. Besides being a globally important source of aerosol particles that could impact clouds, precipitation, and radiation, wildfire activity heats the environment dramatically and can significantly perturb the environmental thermodynamics. However, this impact on environmental thermodynamics and the subsequent convection generated is poorly represented in models. We have developed and evaluated a model capability that accounts for the impact of heat flux from wildfires and is computationally efficient. We have used the new model to explore a pyrocumulonimbus event that occurred in Texas and Oklahoma on 11–12 May 2018 triggered by the Mallard Fire. The simulation accounting for effects of both heat flux and aerosol emissions from the wildfire predicts radar reflectivity, precipitation, hailstone size, and lightning reasonably well based on comparisons with observations. Both the heat flux and aerosol emissions from the wildfire increase low-level temperatures and midlevel thermal buoyancy significantly, causing stronger upward motion that lifts more supercooled water to higher levels. The increase in available supercooled water for hail growth and invigorated updrafts leads to larger hail size and enhanced lightning. The effect of heat flux on storm intensity is considerably more significant than that of aerosol emissions.

1. Introduction

Wildfire frequency and burned area have been increasing in recent decades globally, particularly in the western United States (e.g., Dennison et al., 2014; Miller et al., 2012). It is well known that wildfires can cause substantial increases in the emissions of gases including health-hazardous gas pollutants and greenhouse agents such as carbon monoxide, nitrogen oxides, ozone, and aerosol particles (Liu et al., 2017; Phuleria et al., 2005). Much less is known about the latter than the former effects. Aerosols released from wildfires can affect weather and climate through aerosol-radiation-cloud interactions (Lee et al., 2018; Lindsey & Fromm, 2008; Logan, 2018; Logan et al., 2018; Lu & Sokolik, 2013). Besides the emissions of gases and aerosol particles, they simultaneously release a large amount of heat to the lower and middle troposphere and dramatically impact environmental thermodynamics (Kablick et al., 2018; Trentmann et al., 2006). Large fires also release water vapor as a by-product of combustion, which could affect environmental thermodynamics (Peterson et al., 2016). Pyrocumulonimbus (PyroCb) clouds, a fire-induced variety of deep convection that often rises to the upper troposphere or lower stratosphere (Luderer et al., 2006), can be impacted

by the fire emissions of sensible heat, aerosol particles, and water vapor in a complex way that is still poorly understood due to poor model capability of simulating their combined effects.

PyroCb is associated with a hot surface temperature, strong surface winds, low relative humidity, and deep mixed layer (Clements et al., 2018; Cruz et al., 2012; Fromm et al., 2006, 2012; Lareau & Clements, 2016). This type of deep convective cloud is unique in its microphysical structure for the following reasons: (1) There exist high concentrations of small cloud droplets that result from a large number of cloud condensation nuclei due to the aerosol particles emitted by fire that compete for limited condensable water vapor (Andreae et al., 2004), and (2) these clouds initiate and develop under the vigorous dynamics and thermodynamics induced by the fire itself. The buoyancy generated by the sensible heat of wildfires can produce very strong updrafts (Lareau & Clements, 2017; Tory et al., 2018), which can further enhance the aerosol activation at the cloud base by increasing the supersaturation (Kablick et al., 2018; Luderer et al., 2006; Trentmann et al., 2006). Note that pyroCb often produces severe weather events that include large hail (>25 mm), enhanced lightning activity, extreme low-level winds, and in some cases even tornadoes (Fromm et al., 2006; Lareau et al., 2018; Rosenfeld et al., 2007). PyroCb is also found to produce an anomalously high number of positive lightning, while the lightning produced in ordinary thunderstorms is typically dominated by negative lightning flashes (Jungwirth et al., 2005; Rosenfeld et al., 2007). Positive lightning is often an order of magnitude stronger than negative lightning (Jungwirth et al., 2005). The occurrence of high percentage, high rate, and high density of positive lightning has a direct relationship with storm severity and is coincident with the production of large hail (Logan et al., 2018; Rosenfeld & Woodley, 2000; Wang et al., 2018; Williams et al., 2005).

Previous studies (Kablick et al., 2018; Luderer et al., 2006) simulated the impact of wildfires by changing the initial backgrounds with prescribed heat and aerosol emitted by the wildfire. Modeling of wildfire impact in regional and global climate models (RGCMs) has been difficult because (1) wildfire plume rise is often a complex function of the size of the wildfire, fire heat flux, and the atmospheric environmental conditions, and (2) model grid spacing needs to be very small (e.g., <100 m) to simulate fire dynamics, which is generally not yet affordable in RGCMs. Various schemes for parameterizing plume rise, ranging from simple empirical-based schemes such as Briggs, Sofiev, and DAYSMOKE (Briggs, 1975; Liu et al., 2017; Sofiev et al., 2012) to relatively sophisticated prognostic 1-D parcel models that include cloud microphysics and entrainment (Freitas et al., 2007), have been developed over the years in an effort to determine the injection height of wildfire emissions. There are detailed fire models that can explicitly resolve fire spread and fire plume dynamics, for example, MesoNH-ForeFire (Filippi et al., 2011) and the fire-spread model (SFIRE) that was coupled with Weather Research and Forecasting (WRF; Mandel et al., 2011 and Mandel et al., 2014) and WRF coupled with chemistry (WRF-Chem; Kochanski et al., 2012, 2013). However, such fire models are computationally expensive. For example, the WRF-Chem-SFIRE simulation costs about 50% more than the simulation without SFIRE in the Mallard Fire case that will be discussed in the following section. In addition, it is challenging to run these expensive simulations in weather forecasts and RGCMs. Furthermore, our poor understanding of fire ignition and the limitation on defining variable ignition locations and sources in a detailed fire model could pose a large model uncertainty. Thus, a relatively simplified subgrid plume parameterization is more practical in model applications, particularly considering the computational cost.

In WRF-Chem, the subgrid plume model is represented by embedding a 1-D time-dependent cloud model (Freitas et al., 2007) within each column of WRF-Chem. However, currently the subgrid dispersion is only considered for aerosols emitted from wildfires (Grell et al., 2011). The heat effect of wildfires on environmental thermodynamics has not been considered, which was noted as a potential development area in Grell et al. (2011). At a relatively coarse resolution (e.g., ~30 km), fire burning has a much smaller scale than the model grid, so the heat likely has a small impact on the grid mean temperature. However, in models that run at cloud-resolving and convection-permitting scales (kilometers) at which the grid size is comparable to or even smaller than the burned areas of wildfires, the heat effect of wildfires on grid-scale temperature can become important and should be considered. Therefore, the first goal of this study is to enable WRF_Chem to account for impacts of both aerosols and heat from wildfires without adding obvious computational cost. Second, we will use the new WRF-Chem model to examine the role of the wildfire in altering pyroCb properties including convective intensity, hailstone size, and lightning behavior, as well as the relative importance of the heat impact relative to the aerosol impact. The unique aspects of this study lie in the

development of a new model capability to account for heat effect computational efficiently, the application to a real fire event that was well characterized in a field experiment, and the quantification of the respective heat effect and aerosol effect on convective extremes.

2. Model Development and Evaluation

In order to account for the heat effect of wildfires without adding significant computational cost to the WRF-Chem model (Chapman et al., 2009; Fast et al., 2006), our method is based on the existing subgrid 1-D plume rise model (Freitas et al., 2007). The evolution and injection height of the fire plume is estimated by the 1-D plume rise model originally developed by Latham (1994) at each grid column of the 3-D host model (i.e., WRF-Chem). The final height that the plume reaches is determined by the thermodynamics of the atmospheric environment acquired from the host model and the surface heat flux release from wildfires. All wildfires are aggregated into three categories (forest, woody savanna, and grassland) by merging the fire location with the land use data set. The heat fluxes of different types of wildfires are obtained from the data in Table 1 of Freitas et al. (2006). The heat fluxes used for forest, woody savanna, and grassland are 80, 23, and 3.3 kW/m^2, respectively. The subgrid plume rise model is driven by environmental dynamics from the atmosphere model in WRF-Chem, and the plume dynamics is estimated based on fire information from the Fire INventory from National Center for Atmospheric Research (Freitas et al., 2007). The heat flux from the plume model which assumes an exponential decay with altitude is input to the atmosphere model by being treated as an additional forcing term in the thermodynamics equation of the atmosphere model. This is done in the same way as WRF-SFIRE as described in Mandel et al. (2011). The detailed equation along with other details about fire location, timing, and biomass emissions are provided in the supporting information (SI). Note that, unlike WRF-SFIRE, in which the heat fluxes are calculated by SFIRE, we estimate the heat fluxes in a simple and less expensive way following the equation $\sum_i (HF_i \times BA_i)/\text{grid size}$, where HF_i denotes the heat flux of each fire type and BA_i is the burned area of each type. Thus, no significant computational cost is added.

Our initial evaluation of the new model capability in WRF-Chem uses 3-km resolution for wildfires without pyroCb (see SI for detailed model configuration). Soundings are found at the three locations that have near-surface winds blowing from an adjacent significant wildfire (Figure S1a in the SI). We evaluate the low-level temperature profiles with the radiosonde data. The evaluation shows an environmental temperature increase of roughly 2–3 °C near the surface by accounting for the sensible heat flux from wildfires, leading to a better agreement with observed temperature (Figure S1b).

The WRF-Chem model with the new plume model development is further evaluated at 1-km resolution with observations from a well-observed wildfire event that induced a pyroCb and a corresponding simulation from WRF-Chem-SFIRE, which explicitly simulates fires. The Mallard Fire at the panhandle of Texas, which burned more than 260 km^2, began on the evening of 8 May 2018 and lasted for over 1 week and charred primarily savannah vegetation. The Mallard Fire induced a pyroCb that occurred on 11–12 May 2018 as observed from GOES-16 (Figure S2a). This impressive pyroCb produced both large hailstones (25 mm) and frequent lightning (numerous positive cloud-to-ground [CG] and intracloud [IC] lightning pulses) over the region between Texas and Oklahoma (35.2–35.7°N, 99.5–100.5°W). The baseline simulation includes the impact of both heat flux and aerosol emissions using the new plume model and is referred to as Wildfire. The WRF-Chem-SFIRE simulation uses the same model setup as Wildfire. The simulations are conducted at 1-km resolution over a domain shown in Figure S2a. The simulations are initiated at 0000 UTC on 9 May and run out to 0000 UTC on 14 May 2018. More detailed information about the simulations are described in the SI. To examine temperature anomalies induced by the fires in Wildfire and WRF-Chem-SFIRE, we conduct an additional WRF-Chem simulation in which both the heat flux and aerosol emissions from the wildfire are turned off (referred to as No_Wildfire).

The fire burned area simulated in Wildfire (black box in Figure 1a) on 11 May is ~300 km^2, which is similar to the burned area in WRF-Chem-SFIRE (black box in Figure 1b). The heat fluxes from the Mallard Fire averaged over the fire burned area during 1200–1800 UTC on 11 May 2018 (several hours before the pyroCb) simulated by Wildfire have a range of 10–23 kW/m^2 (Figure 1a) with a mean of ~18.7 kW/m^2, which is a slight underestimate of ~20.3 kW/m^2, the corresponding mean value from WRF-Chem-SFIRE

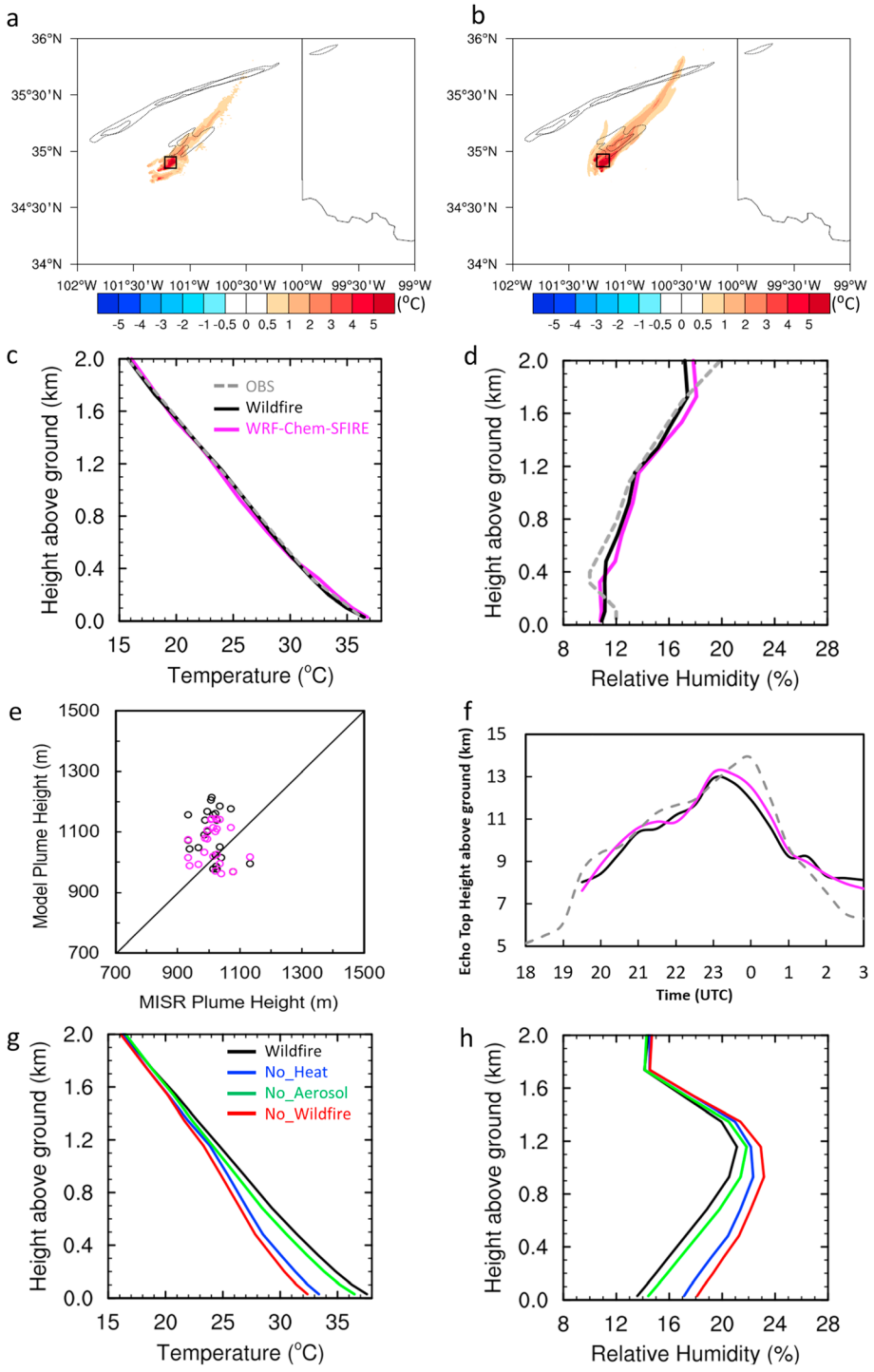

Figure 1. (a) Temperature anomaly at 2-m altitude (shaded) due to the Mallard Fire simulated by Wildfire by comparing with No_Wildfire at 1800 UTC on 11 May (2 hr before the initiation of convection). Black boxes denote the fire burned areas. The composite reflectivity (dotted contour lines; 10 and 20 dBZ for the outer and inner cycles, respectively) at 2000 UTC is overlaid to show the connection of the temperature anomaly with the pyrocumulonimbus. (b) The same as (a), except for WRF-Chem-SFIRE. The profiles of (c) temperature and (d) relative humidity at 0000 UTC on 11 May at KAMA from the sounding (gray dashed), Wildfire (black solid), and WRF-Chem-SFIRE (magenta solid). (e) Comparison of plume heights among MISR, Wildfire (black circles), and WRF-Chem-SFIRE (magenta circles) during 1730–1800 UTC on 13 May. (f) Comparison of radar echo top heights averaged over the red box in Figure S2a among the Next-Generation Weather Radar observation (gray dashed), Wildfire (black solid), and WRF-Chem-SFIRE (magenta solid). The echo top heights are defined with the threshold of reflectivity of 0 dBZ. (g and h) The temperature and relative humidity profiles at 1800 UTC on 11 May at the Mallard fire area (yellow box in Figure S2a) from Wildfire (black), No_Heat (blue), No_Aerosol (green), and No_Wildfire (red). WRF-Chem-SFIRE = Weather Research and Forecasting coupled with chemistry/fire-spread model; MISR = Multi-angle Imaging Spectro Radiometer.

(Figure 1b). Wildfire and WRF-Chem-SFIRE simulate similar temperature perturbations near the surface over the fire area and the downwind regions 2 hr before the pyroCb is initiated, which exceeds 5 °C at Mallard (Figures 1a and 1b).

We also evaluate Wildfire and WRF-Chem-SFIRE with a sounding from the Amarillo, TX (KAMA) site. It is evident that the KAMA site was indeed influenced by a small fire near Amarillo (~7 km to the south; shown as a red dot adjacent to the white dot in Figure S2c) on 10 May due to the southwesterly winds at low levels (Figure S2d). Overall, Wildfire predicts the temperature and relative humidity that are consistent with the sounding data at 0000 UTC on 11 May at KAMA (Figures 1c and 1d). The results are very similar to those in WRF-Chem-SFIRE. Wildfire generally overestimates plume heights by 100–300 m (Figure 1e), which is within the measurement uncertainty range of about ±500 m (Martin et al., 2018). WRF-Chem-SFIRE agrees with the observations slightly better. The 0-dBZ echo top height from Wildfire is very similar to WRF-Chem-SFIRE (Figure 1f), with the maximum value occurring roughly 1 hr earlier and underestimated by ~1 km in comparison to the observations from Next-Generation Weather Radar (NEXRAD) network. The computational cost of the WRF-Chem-SFIRE simulation is about 45% more than Wildfire. Those validations show that our new development can capture the heat effects from the fires in a similar way as the detailed fire simulation from SFIRE but more computationally efficient, which is more applicable to weather forecast and RGCMs.

Note that the simulations for all above evaluations are driven by Rapid Refresh (RAP) reanalysis data, which assimilates various observational data, including radar, satellite, and radiosondes (Benjamin et al., 2016). Both the KAMA sounding and NEXRAD data were used for data assimilation in RAP; it is fair to say that part of the heat impact from the wildfires is already accounted for. This is a model dilemma: Without being driven by reanalysis data, real-case model simulations can be unsuccessful; therefore, it is difficult to use observations to evaluate model fidelity. On the other hand, the use of the reanalysis data may lead to an underestimation of the heat effect. The underestimation of the heat effect will be further estimated in the last section.

We then apply the WRF-Chem with the new plume model to study the impact of wildfire on the pyroCb. We mainly consider the effects of heat and aerosol emissions from the wildfire since water vapor was found to contribute little to the intensity of convection (Lee et al., 2018; Trentmann et al., 2006). In addition to Wildfire and No_Wildfire simulations, we conduct the following sensitivity tests: (a) No_Heat, in which the heat fluxes from the wildfire is turned off based on Wildfire; (b) No_Aerosol, in which the aerosol emission from the wildfire is turned off based on Wildfire; and (c) No_PBLheat, which is based on No_Heat except the upward sensible heat flux from planetary boundary layer (PBL) is disabled.

3. Wildfire Impacts on PyroCb

Figures 1g and 1h show that, in Wildfire, the near surface temperature over the Mallard fire area (no sounding data available) was high (~37.5 °C) with a low relative humidity (~13.5%) 2 hr prior to convective initiation. Note the terrain height is about 1.1 km over the area. By comparing Wildfire with No_Wildfire, the wildfire contributes to the remarkable increase in temperature (~4 °C at 0.4 km and ~5.5 °C near the surface; Figure 1g) and the decrease in relative humidity (from 18% to 13.5% near surface; Figure 1h). As expected, the temperatures are similar among different simulations at site A where there is not much of a wildfire influence (Figure S2b). The heat effect warms the lower atmosphere substantially (~4.5 °C near the surface; Figure 1g). However, the aerosol effect only slightly warms the atmosphere (~1 °C near the surface), as a result of absorbing radiation by smoke aerosols. Note that the difference in relative humidity is mainly due to the change in temperature since the water vapor mixing ratio does not differ much between the simulations.

The impacts of the Mallard wildfire on precipitation, hail, and lightning are shown in Figures 2, S3, and S4). Changes from Wildfire to No_Wildfire include the reduced occurrences in convective rain rates (>15 mm/hr), extreme hailstone sizes (>20 mm), and very high reflectivity (>55 dBZ; Figure 2). The lightning stroke rates are reduced by ~40%. These results suggest the wildfires substantially increase the severity of the convective storm. In fact, the convective intensity is markedly enhanced when the full effects of the wildfire are considered (Figure 3a). The Wildfire simulation reproduces well the 6-hr accumulated precipitation as observed from 2000 UTC on 11 May to 0200 UTC on 12 May (Figures S3a and S3b), except for a northwestward shift of the location of heavy rain. The hourly precipitation rate in Wildfire has the highest occurrence probability in the range of 15–20 mm/hr, which also shows the best agreement with the observations

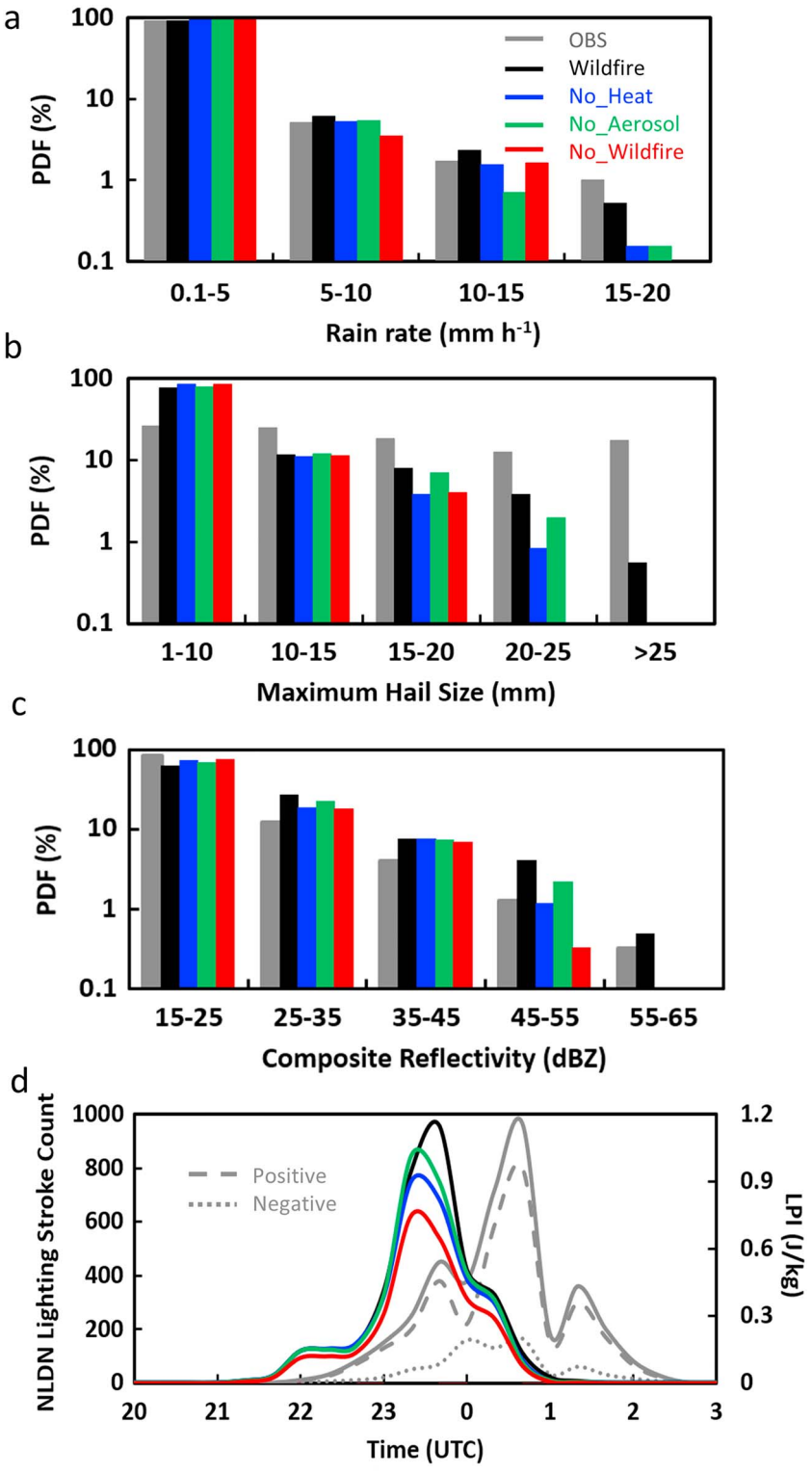

Figure 2. PDFs of (a) rain rates (>0.1 mm), (b) maximum hail size (>1 mm), and (c) composite reflectivity (>15 dBZ) from 2000 UTC on 11 May to 0200 UTC on 12 May when the pyrocumulonimbus occurs. The value in the parentheses is the threshold applied to the data for the PDF calculation. (d) Time series of total lightning stroke (IC + CG) from NLDN (gray dashed line for the total [IC + CG] positive lightning and gray dotted line for the total negative lightning) and the Lightning Potential Index (LPI) from the simulations. The observed maximum hail size is from the maximum expected size of hail data. The analysis domain is the red box marked in Figure S2a. PDF = probability density function; IC = intracloud; CG = cloud-to-ground; NLDN = National Lightning Detection Network.

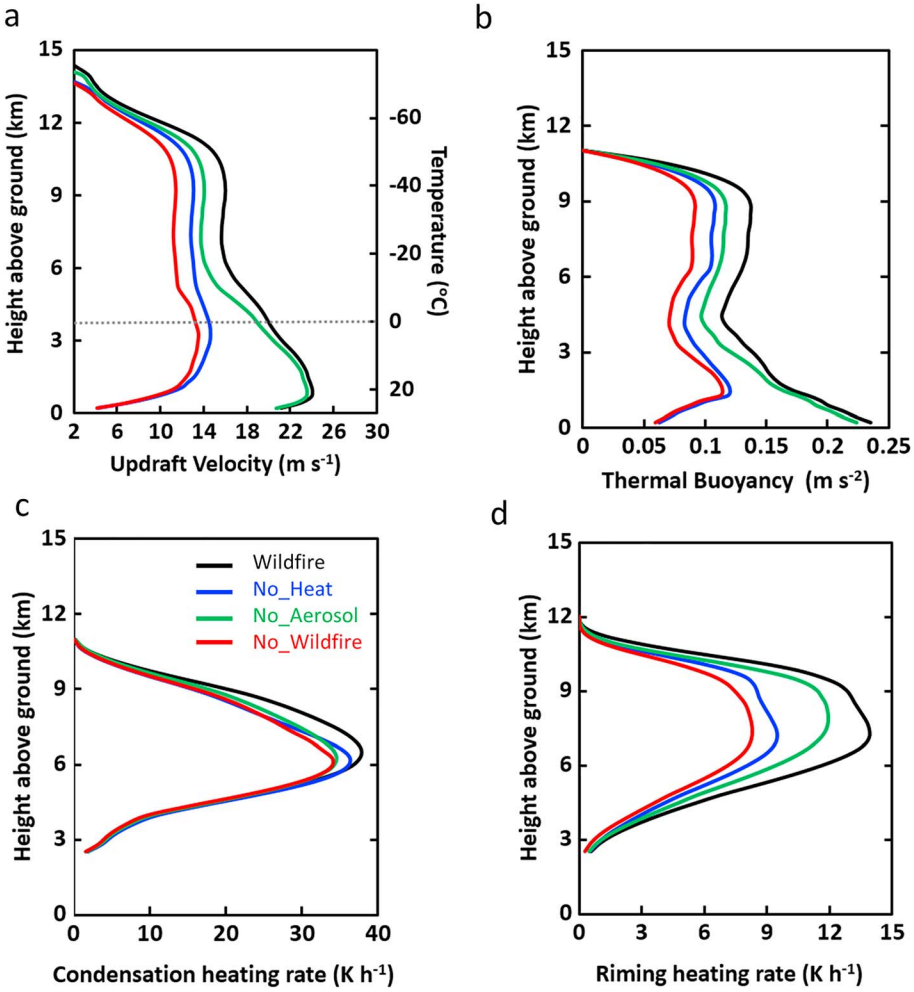

Figure 3. Vertical profiles of (a) updraft velocity, (b) thermal buoyancy, (c) condensation heating rate, and (d) riming heating rate averaged over the top 25 percentiles (i.e., 75th to 100th) of the updrafts with $w > 2$ m/s from the simulations during the convection period from 2000 UTC on 11 May to 0000 UTC on 12 May over the analysis domain as shown in the red box in Figure S2a. The dotted line in (a) denotes the freezing level (0 °C).

(Figure 2a). The simulated composite reflectivities (i.e., the column maximum) are up to 55–65 dBZ, which are consistent with the presence of hail, and agree with NEXRAD (GridRad; Homeyer & Bowman, 2017). In addition, Wildfire captures a similar region for hail occurrence as observed from both Storm Prediction Center reports and maximum expected size of hail (MESH; Figures S4a and S4b) and simulates the largest hail size of ~26 mm, which is in agreement with the reported 25.4 mm from the Storm Prediction Center but ~10 mm smaller than that from the radar-retrieved MESH. The MESH data used in this study are developed from a newly improved algorithm (Murillo & Homeyer, 2019) and generally has an uncertainty of ±7 mm. Without considering the wildfire impacts, No_Widlfire underestimates the accumulated precipitation by ~30% (Figures S3b vs. S3e) and the heavy rain rates do not occur (Figure 2a). Also, the hail region shrinks, and the maximum hail size decreases to 18 mm (Figures S4b vs. S4e). The observation shows the lightning flash rate maximum of ~200 flashes/min where most of those flashes are positive IC pulses (compare Figure 2d with Figure S5). On the other hand, the CG flash rate is much lower than IC especially for positive CG flashes (<2 flashes/min; Figure S5), which suggests an absence of the dynamic forcing needed to produce the high positive CG flash rates typically observed in polluted deep convective clouds (Logan et al., 2018; Lyons et al., 1998; Rosenfeld et al., 2007; Wang & Zhang, 2009). The modeled Lightning Potential Index (LPI) from Wildfire peaks about 1 kh ahead of the observed peak that is at 0030 UTC on 12 May in lightning flashes (Figure 2d). Without the wildfire effect, LPI is drastically reduced by ~40%.

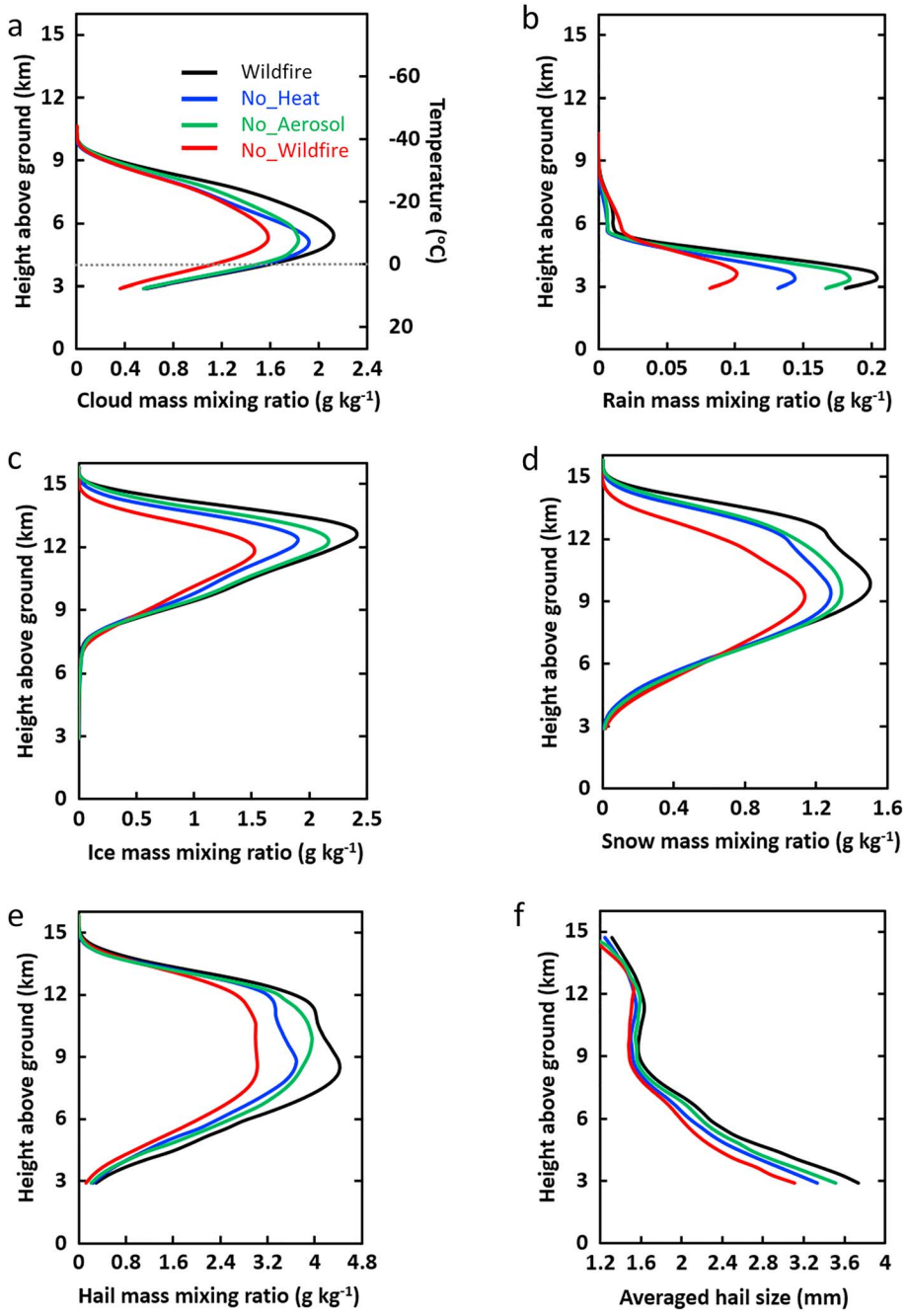

Figure 4. Vertical profiles of mass mixing ratios for (a) cloud, (b) rain, (c) ice, (d) snow, (e) hail, and mean hail size for (f) hail averaged over the top 25 percentiles (i.e., 75th to 100th) of the updrafts with $w > 2$ m/s from the simulations during the strong precipitation and lightning period from 2300 UTC on 11 May to 0000 UTC on 12 May over the analysis domain as shown in the red box in Figure S2a. The dotted line in (a) denotes the freezing level (0 °C).

Both No_Heat and No_Aerosol underestimate the 6-hr total precipitation by ~3 mm and the frequency of rain rates larger than 10 mm/hr (Figures S3c, S3d, and 2a). The relative significance of the heat effect on precipitation is similar to the aerosol effect. Both the sensible heat and aerosol effects of the wildfire contribute to higher reflectivity, larger hail size, and higher lightning potential. However, the sensible heat impact is more evident. The frequency of high reflectivity (>45 dBZ) is reduced to ~4% in No_Aerosol and ~1% in No_Heat from 7% in Wildfire (Figure 2c). The maximum hail size decreases by ~4 mm when neglecting the aerosol effect and by ~6 mm when neglecting the heat effect (Figure S4). The LPI maximum is

reduced by ~25% in No_Heat and ~15% in No_Aerosol (Figure 2d). Taking both factors into account, the maximum hail size decreases by ~8 mm from Wildfire to No_Wildfire simulation. The mutual effect of heat and aerosols from wildfires on hail size is less than the sum of the respective effect from both factors, indicating a nonlinear damping effect on the hail size when the two factors work together.

We now explain how the wildfire enhances convective extremes (larger precipitation and reflectivity, extreme hailstone size, and more lightning). As shown in Figure 3a, the wildfire markedly invigorates convection, which can be explained by the increased thermal buoyancy from the subcloud to cloud regime (Figure 3b). Note that there is an appreciable subcloud vertical velocity (below 3 km) in Wildfire and No_aerosol, about 4–6 times larger compared with No_Heat and No_Widlfire, which is consistent with large subcloud vertical velocity in a developing pyroCb plume observed in Clements et al. (2018). This large subcloud vertical velocity appears before and at the initial stage of the pyroCb storm (Figure S6), a result of the sensible heating due to the heat released from wildfires. At the high levels after storm is initiated, latent heating because of cloud microphysics is another reason for the increased thermal buoyancy in Wildfire compared with No_Wildfire. We find that the two major microphysical processes that dominate the latent heating are condensation and riming as shown in Figures 3c and 3d, respectively. The wildfire leads to an increase in latent heating by ~4 K/hr through condensation and ~6 K/hr through riming. After 2130 UTC as storm develops deeper, latent heating plays a more significant role; therefore, aerosol effect on updraft velocity is shown clearly (Figure S6). Overall during the strong precipitation and lightning period from 2300 UTC on 11 May to 0000 UTC on 12 May, the respective heat effect leads to ~25% increase in the vertical maximum of the averaged profile of top 25 percentiles of updraft speeds, while the aerosol effect leads to ~15% increase. By comparing with the ~50% enhancement due to the combined effect, the mutual effects of heat and aerosol from the wildfire have nonlinear amplification effects on convective intensity.

The larger hail and cloud electrical activity are likely due to a larger amount of supercooled water content from No_Wildfire to Wildfire (~40% more; Figure 4a). The droplet number concentrations are doubled from the cloud base that is at 3.5–4 km above the surface (Figure S7a). It is interesting to note that No_Aerosol even has higher supercooled cloud droplet number and mass mixing ratios compared with No_Heat above 8 km, despite a much smaller droplet number concentration at low levels as a result of lower aerosol number concentrations, indicating that the stronger updrafts in No_Aerosol (Figure 3a) lift more cloud droplets to the high levels. This shows the important role of updraft intensity that is enhanced by the heat effect in producing supercooled water at high levels. Mainly through riming, more supercooled droplets participate in forming more ice, snow, and hail, thereby releasing a large amount of heat aloft (Figures 4c–4e and S7c–S7ce). It is known that larger amount of supercooled water available for accretion at subfreezing temperatures boosts the hail growth rate in cloud updrafts (Ilotoviz et al., 2018). In addition, the stronger updrafts provide more time for sufficient growth of a hailstone in its favored growth region (Guo & Huang, 2002), ultimately leading to larger hail size. As a result, both hail mass and number are increased (by ~45% and ~27%, respectively) by the wildfire (Figures 4e and S7e), with the mean hail size increased by ~25% (Figure 4f).

Lightning forms from the noninductive charge separation caused by collisions between ice particles in the presence of supercooled liquid water within strong updrafts (Takahashi & Miyawaki, 2002). In the absence of strong dynamic forcing (e.g., a front or outflow boundary) in this case, the sensible heat helps air parcel overcome the large amount of surface-based convective inhibition (~220 J/kg) by increasing the surface heat flux and updraft strength. The aerosols from wildfires further invigorate convection through enhanced latent heating from condensation and riming as shown in Figures 3c and 3d (Fan et al., 2018; Rosenfeld et al., 2008). In addition, the aerosols increase supercooled droplets evidently. Therefore, the combination of sensible heat flux and aerosol loading contribute to the overall enhanced electrical activity of the pyroCb from No_Wildfire to Wildfire. Compared with the aerosol effect, the heat effect from wildfire contributes more significantly to developing larger hail size and more lightning, mainly because of stronger convective intensity and more supercooled droplets resulting from stronger vertical transport.

4. Summary and Discussion

We have developed a computationally efficient model capability to account for heat flux from wildfires in the WRF-Chem model. Using a combination of observations and a detailed fire module (i.e., SFIRE) for evaluation, the new model improves the simulation of temperature profiles at low levels and simulates the fire-

related properties (e.g., temperature perturbation, heat fluxes, and plume height) consistent with the explicit fire simulation that requires approximately 45% more computation time than our new model simulation in the test case. This indicates a practical application of our new model development to weather and climate models to account for the impact of heat fluxes released from wildfires on atmospheric thermodynamics. We applied the new model to explore the impacts of the Mallard wildfire on the severity of a rare mesocyclonic pyroCb event occurring in Texas and Oklahoma on 11–12 May 2018, which is unique in the North American inventory of pyroCb, and examined the total and individual contributions by heat flux and aerosol emissions from the wildfire to the pyroCb properties.

The simulation accounting for both sensible heat flux and aerosol emissions from the wildfire reproduces reflectivity, precipitation, maximum hail size, and lightning, showing better agreements with observations than the simulations that do not account for either heat or aerosol emissions. Both heat and aerosols emitted from the wildfire increase low-level temperatures and enhance frequencies of extreme precipitation rate (>15 mm/hr), high reflectivity (>55 dBZ), large hailstone size (>20 mm), and lightning potential. Even with a background meteorology where part of heat effect is already accounted for, the heat effect is more significant than the aerosol effect in enlarging maximum hail size by ~6 mm more and enhancing lightning potential by ~20%. We also see a role of aerosols in enhancing convective intensity (through increased latent heat release by condensation and riming) and the frequency of heavy precipitation rates. The effect of the wildfire on convective intensity is remarkable (a 50% increase in the mean of top 25 percentiles of updraft speed during the strong precipitation and lightning period), which is solely contributed by the added heat from the wildfire at the initial stage of the storm with a noticeable role of aerosol in increasing latent heating as storm developing. The intensified updrafts lift more liquid condensate to the higher levels and produce a larger amount of supercooled water, enhancing hail growth and resulting in larger hailstones. The larger ice particles in the presence of more supercooled liquid within stronger updraft can enhance positive lightning, which may explain the large portion of positive IC lightning flash rate in the observations but not necessarily the positive CG lightning flash rate that is typically observed in polluted deep convective clouds. It is interesting to note that when the two factors are considered together, there is a nonlinear amplification effect on the intensity of convection compared with their respective singular effects but a nonlinear damping effect on hail size. The nonlinear amplification effect on convective intensity suggests that aerosol invigoration through enhancing latent heat release may be more significant for stronger storms compared with weaker ones.

Although we demonstrate that the heat effect from the wildfire contributes significantly to pyroCb initiation, intensity, and consequently severe weather (i.e., hail and lightning), the heat effect in our study is still underestimated because the initial and boundary meteorological conditions from RAP have accounted for some heat impact due to the assimilation of the KAMA sounding and NEXRAD radar data in RAP. This is also evidenced from the fact that convection still occurs in No_Wildfire. Based on the sounding at KAMA at 1200 UTC on 11 May (about 8 hr before the initiation of convection), there is a stout capping inversion with no convective available potential energy along with positive value for the lifted index, suggesting the environment was not conducive to convection in the morning (Figure S8a). In the afternoon, the environment may become less adverse to convection, but unfortunately there is no sounding data to validate it. To corroborate the key role of the heat flux in triggering the convection, we have conducted another sensitivity test No_PBLheat based on No_Heat by removing the PBL heat tendency. This is to completely exclude the heat effect from the surface and PBL. No pyroCb occurs in this simulation, and the temperatures below 300 m are about ~1.5–2 °C lower compared with No_Wildfire (Figures S8b and S8c). This suggests the heat impact on the environmental temperature could be underestimated by up to ~1.5–2 °C.

It should be noted that in our development, the heat is added as a source term impacting grid-scale temperature, similar to the treatment in WRF-SFIRE. Whether the added capability can trigger pyroCb or not depends on host model resolution and atmospheric conditions. In this study, with 1-km grid spacing and an environmental temperature close to the convective temperature, the pyroCb is triggered and is well simulated.

Acknowledgments
This study is supported by the U.S. Department of Energy Office of Science Early Career Award Program. PNNL is operated for the U.S. Department of Energy (DOE) by Battelle Memorial Institute undercontract DE-AC05-76RL01830. Zhanqing Li acknowledges the support of NASA Grant (NNX16AN61G). NOAA/ESRL radiosonde date are from the https://ruc.noaa.gov/raobs/ website. The NCEP Stage IV precipitation data are from the https://www.emc.ncep.noaa.gov/mmb/ylin/pcpanl/stage4/ website. The MISR data are obtained from the https://misr.jpl.nasa.gov/getData/accessData/ website. The NEXRAD and MESH data were produced by coauthor Cameron Homeyer and available online (http://gridrad.org/). The NOAA SPC report data are available from the https://www.spc.noaa.gov/climo/online/ website. The NLDN lightning data are obtained through Ronald Holle at Vaisala, Inc (https://my.vaisala.net/en/services/dataservicesandsolutions/lightningdata/Pages/NLDN.aspx). Model simulation data are available at our project website (http://portal.nersc.gov/project/m2977/wildfire_grl).

References

Andreae, M. O., Rosenfeld, D., Artaxo, P., Costa, A. A., Frank, G. P., Longo, K. M., & M. A. F. (2004). Silva-Dias, Smoking rain clouds over the Amazon. *Science*, *303*(5662), 1337–1342. https://doi.org/10.1126/science.1092779

Benjamin, S. G., Weygandt, S. S., Brown, J. M., Hu, M., Alexander, C. R., Smirnova, T. G., et al. (2016). A North American hourly assimilation and model forecast cycle: The rapid refresh. *Monthly Weather Review*, *144*(4), 1669–1694. https://doi.org/10.1175/MWR-D-15-0242.1

Briggs, G. A. (1975). In D. A. Haugen (Ed.), *Plume rise predictions. In Lectures on air pollution and environmental impact analyses*, (Vol. 1975, pp. 59–111). Boston, MA, USA: American Meteorological Society.

Chapman, E. G., Gustafson, W. I. Jr., Easter, R. C., Barnard, J. C., Ghan, S. J., Pekour, M. S., & Fast, J. D. (2009). Coupling aerosol-cloud-radiative processes in the WRF-Chem model: Investigating the radiative impact of elevated point sources. *Atmospheric Chemistry and Physics*, *9*(3), 945–964. https://doi.org/10.5194/acp-9-945-2009

Clements, C. B., Lareau, N., Kingsmill, D. E., Bowers, C. L., Camacho, C. P., Bagley, R., & Davis, B. (2018). RaDFIRE—The Rapid Deployments to Wildfires Experiment (RaDFIRE): Observations from the fire zone. *Bulletin of the American Meteorological Society*, *99*(12), 2539–2559. https://doi.org/10.1175/BAMS-D-17-0230.1

Cruz, M. G., Sullivan, A. L., Gould, J. S., Sims, N. C., Bannister, A. J., Hollis, J. J., & Hurley, R. J. (2012). Anatomy of a catastrophic wildfire: The Black Saturday Kilmore East fire in Victoria, Australia. *Forest Ecology and Management*, *284*, 269–285. https://doi.org/10.1016/j.foreco.2012.02.035

Dennison, P. E., Brewer, S. C., Arnold, J. D., & Moritz, M. A. (2014). Large wildfire trends in the western United States, 1984–2011. *Geophysical Research Letters*, *41*, 2928–2933. https://doi.org/10.1002/2014GL059576

Fan, J., Rosenfeld, D., Zhang, Y., Giangrande, S. E., Li, Z., Machado, L. A. T., et al. (2018). Substantial convection and precipitation enhancements by ultrafine aerosol particles. *Science*, *359*(6374), 411–418. https://doi.org/10.1126/science.aan8461

Fast, J. D., Gustafson, W. I. Jr., Easter, R. C., Zaveri, R. A., Barnard, J. C., Chapman, E. G., et al. (2006). Evolution of ozone, particulates, and aerosol direct radiative forcing on the vicinity of Houston using a fully coupled meteorology-chemistry-aerosol model. *Journal of Geophysical Research*, *111*, D21305. https://doi.org/10.1029/2005JD006721

Filippi, J. B., Bosseur, F., Pialat, X., Santoni, P., Strada, S., & Mari, C. (2011). Simulation of coupled fire/atmosphere interaction with the MesoNH-ForeFire models. *Journal of Combustion*, *2011*, 1–13. https://doi.org/10.1155/2011/540390

Freitas, S. R., Longo, K. M., & Andreae, M. O. (2006). Impact of including the plume rise of vegetation fires in numerical simulations of associated atmospheric pollutants. *Geophysical Research Letters*, *33*, L17808. https://doi.org/10.1029/2006GL026608

Freitas, S. R., Longo, K. M., Chatfield, R., Latham, D., Silva Dias, M. A. F., Andreae, M. O., et al. (2007). Including the sub-grid scale plume rise of vegetation fires in low resolution atmospheric transport models. *Atmospheric Chemistry and Physics*, *7*(13), 3385–3398. https://doi.org/10.5194/acp-7-3385-2007

Fromm, M. D., McRae, R. H. D., Sharples, J. J., & Kablick, G. P. III (2012). Pyrocumulonimbus pair in Wollemi and Blue Mountains National Parks, 22 November 2006. *Australian Meteorological and Oceanographic Journal*, *62*, 117–126.

Fromm, M. D., Tupper, A., Rosenfeld, D., Servranckx, R., & McRae, R. (2006). Violent pyro-convective storm devastates Australia's capital and pollutes the stratosphere. *Geophysical Research Letters*, *33*, L05815. https://doi.org/10.1029/2005GL025161

Grell, G., Freitas, S. R., Stuefer, M., & Fast, J. (2011). Inclusion of biomass burning in WRF-Chem: Impact of wildfires on weather forecasts. *Atmospheric Chemistry and Physics*, *11*(11), 5289–5303. https://doi.org/10.5194/acp-11-5289-2011

Guo, X., & Huang, M. (2002). Hail formation and growth in a 3D cloud model with hail-bin microphysics. *Atmospheric Research*, *63*(1-2), 59–99. https://doi.org/10.1016/S0169-8095(02)00019-4

Homeyer, C. R., & Bowman, K. P. (2017), Algorithm description document for version 3.1 of the Three-Dimensional Gridded NEXRAD WSR-88D Radar (GridRad) dataset. Available online at: http://gridrad.org/pdf/GridRad-v3.1-Algorithm-Description.pdf.

Ilotoviz, E., Khain, A., Ryzhkov, A. V., & Snyder, J. C. (2018). Relationship between aerosols, hail microphysics, and Z_{DR} columns. *Journal of the Atmospheric Sciences*, *75*(6), 1755–1781. https://doi.org/10.1175/JAS-D-17-0127.1

Jungwirth, P., Rosenfeld, D., & Buch, V. (2005). A possible new molecular mechanism of thundercloud electrification. *Atmospheric Research*, *76*(1-4), 190–205. https://doi.org/10.1016/j.atmosres.2004.11.016

Kablick, G. P., Fromm, M. D., Miller, S. D., Partain, P., Peterson, D., Lee, S. S., et al. (2018). The Great Slave Lake pyroCb of 5 August 2014: Observations, simulations, comparisons with regular convection, and impact on UTLS water vapor. *Journal of Geophysical Research: Atmospheres*, *123*, 12,332–12,352. https://doi.org/10.1029/2018JD028965

Kochanski, A. K., Beezley, J. D., Mandel, J., & Kim, M. (2012). WRF fire simulation coupled with a fuel moisture model and smoke transport by WRF-Chem, 13th WRF Users' Workshop, National Center for Atmospheric Research, 20–24 June 2012, arXiv:1208.1059.

Kochanski, A. K., Jenkins, M. A., Sun, R., Krueger, S., Abedi, S., & Charney, J. (2013). The importance of low-level environmental vertical wind shear to wildfire propagation: Proof of concept. *Journal of Geophysical Research: Atmospheres*, *118*, 8238–8252. https://doi.org/10.1002/jgrd.50436

Lareau, N. P., & Clements, C. B. (2016). Environmental controls on pyrocumulus and pyrocumulonimbus initiation and development. *Atmospheric Chemistry and Physics*, *16*(6), 4005–4022. https://doi.org/10.5194/acp-16-4005-2016

Lareau, N. P., & Clements, C. B. (2017). The mean and turbulent properties of a wildfire convective plume. *Journal of Applied Meteorology and Climatology*, *56*(8), 2289–2299. https://doi.org/10.1175/JAMC-D-16-0384.1

Lareau, N. P., Nauslar, N. J., & Abatzoglou, J. T. (2018). The Carr fire vortex: A case of pyro-tornadogenesis? *Geophysical Research Letters*, *45*, 13–107. https://doi.org/10.1029/2018GL080667

Latham, D. (1994). PLUMP: A one-dimensional plume predictor and cloud model for fire and smoke managers, General technical report INT-GTR-314, Intermountain Research Station, USDA Forest Service, Nov 1994.

Lee, H., Jeong, S.-J., Kalashnikova, O., Tosca, M., Kim, S.-W., & Kug, J.-S. (2018). Characterization of wildfire-induced aerosol emissions from the Maritime Continent peatland and Central African dry savannah with MISR and CALIPSO aerosol products. *Journal of Geophysical Research: Atmospheres*, *123*, 3116–3125. https://doi.org/10.1002/2017JD027415

Lindsey, D. T., & Fromm, M. (2008). Evidence of the cloud lifetime effect from wildfire-induced thunderstorms. *Geophysical Research Letters*, *35*, L22809. https://doi.org/10.1029/2008GL035680

Liu, X., Huey, L. G., Yokelson, R. J., Selimovic, V., Simpson, I. J., Müller, M., et al. (2017). Airborne measurements of western U.S. wildfire emissions: Comparison with prescribed burning and air quality implications. *Journal of Geophysical Research: Atmospheres*, *122*, 6108–6129. https://doi.org/10.1002/2016JD026315

Logan, T. (2018). Anomalous lightning behavior during the 26–27 August 2007 northern Great Plains severe weather event. *Journal of Geophysical Research: Atmospheres*, *123*, 1771–1784. https://doi.org/10.1002/2017JD027750

Logan, T., Dong, X., & Xi, B. (2018). Aerosol properties and their impacts on surface CCN at the ARM Southern Great Plains site during the 2011 Midlatitude Continental Convective Clouds Experiment. *Advances in Atmospheric Sciences*, *35*(2), 224–233. https://doi.org/10.1007/s00376-017-7033-2

Lu, Z., & Sokolik, I. N. (2013). The effect of smoke emission amount on changes in cloud properties and precipitation: A case study of Canadian boreal wildfires of 2007. *Journal of Geophysical Research: Atmospheres*, *118*, 11,777–11,793. https://doi.org/10.1002/2013JD019860

Luderer, G., Trentmann, J., Winterrath, T., Textor, C., Herzog, M., Graf, H. F., & Andreae, M. O. (2006). Modeling of biomass smoke injection into the lower stratosphere by a large forest fire (Part II): Sensitivity studies. *Atmospheric Chemistry and Physics*, *6*(12), 5261–5277. https://doi.org/10.5194/acp-6-5261-2006

Lyons, W. A., Uliasz, M., & Nelson, T. E. (1998). Large peak current cloud-to-ground lightning flashes during the summer months in the contiguous United States. *Monthly Weather Review*, *126*(8), 2217–2233. https://doi.org/10.1175/1520-0493(1998)126<2217:LPCCTG>2.0.CO;2

Mandel, J., Amram, S., Beezley, J. D., Kelman, G., Kochanski, A. K., Kondratenko, V. Y., et al. (2014). Recent advances and applications of WRF–SFIRE. *Natural Hazards and Earth System Sciences*, *14*, 2829–2845.

Mandel, J., Beezley, J. D., & Kochanski, A. K. (2011). Coupled atmosphere-wildland fire modeling with WRF 3.3 and SFIRE 2011. *Geoscientific Model Development*, *4*, 591–610.

Martin, M., Kahn, R. A., & Tosca, M. G. (2018). A global analysis of wildfire smoke injection heights derived from space-based multi-angle imaging. *Remote Sensing*, *10*, 1609. https://doi.org/10.3390/rs10101609

Miller, J. D., Skinner, C. N., Safford, H. D., Knapp, E. E., & Ramirez, C. M. (2012). Trends and causes of severity, size, and number of fires in northwestern California, U.S.A. *Ecological Applications*, *22*(1), 184–203.

Murillo, E. M., & Homeyer, C. R. (2019). Severe hail fall and hail storm detection using remote sensing observations. *Journal of Applied Meteorology and Climatology*, *58*(5), 947–970. https://doi.org/10.1175/JAMC-D-18-0247.1

Peterson, D., Hyer, E. J., Campbell, J. R., Solbrig, J. E., & Fromm, M. D. (2016). A conceptual model for development of intense pyrocumulonimbus in western North America. *Monthly Weather Review*, *145*, 2235–2255.

Phuleria, H. C., Fine, P. M., Zhu, Y., & Sioutas, C. (2005). Air quality impacts of the October 2003 Southern California wildfires. *Journal of Geophysical Research*, *110*, D07S20. https://doi.org/10.1029/2004JD004626

Rosenfeld, D., Fromm, M., Trentmann, J., Luderer, G., Andreae, M. O., & Servranckx, R. (2007). The Chisholm firestorm: Observed microstructure, precipitation and lightning activity of a pyro-cumulonimbus. *Atmospheric Chemistry and Physics*, *7*(3), 645–659. https://doi.org/10.5194/acp-7-645-2007

Rosenfeld, D., Lohmann, U., Raga, G. B., O'Dowd, C. D., Kulmala, M., Fuzzi, S., et al. (2008). Flood or drought: How do aerosols affect precipitation? *Science*, *321*, 1309–1313, 5894, DOI: https://doi.org/10.1126/science.1160606

Rosenfeld, D., & Woodley, W. L. (2000). Deep convective clouds with sustained supercooled liquid water down to −37.5_C. *Nature*, *405*(6785), 440–442. https://doi.org/10.1038/35013030

Sofiev, M., Ermakova, T., & Vankevich, R. (2012). Evaluation of the smoke-injection height from wild-land fires using remote-sensing data. *Atmospheric Chemistry and Physics*, *12*(4), 1995–2006. https://doi.org/10.5194/acp-12-1995-2012

Takahashi, T., & Miyawaki, K. (2002). Reexamination of riming electrification in a wind tunnel. *Journal of the Atmospheric Sciences*, *59*(5), 1018–1025. https://doi.org/10.1175/1520-0469(2002)059<1018:ROREIA>2.0.CO;2

Tory, K. J., Thurston, W., & Kepert, J. D. (2018). Thermodynamics of pyrocumulus: A conceptual study. *Monthly Weather Review*, *146*(8), 2579–2598. https://doi.org/10.1175/MWR-D-17-0377.1

Trentmann, J., Luderer, G., Winterrath, T., Fromm, M. D., Servranckx, R., Textor, C., et al. (2006). Modeling of biomass smoke injection into the lower stratosphere by a large forest fire (Part I): Reference simulation. *Journal of the Atmospheric Sciences*, *6*(12), 5247–5260. https://doi.org/10.5194/acp-6-5247-2006

Wang, Q., Li, Z., Guo, J., Zhao, C., & Cribb, M. (2018). The climate impact of aerosols on the lightning flash rate: Is it detectable from long-term measurements? *Atmospheric Chemistry and Physics*, *18*(17), 12,797–12,816. https://doi.org/10.5194/acp-18-12797-2018

Wang, X., & Zhang, X. (2009). Calculation of electromagnetic induction inside a wind turbine tower struck by lightning. *Wind Energy*, *13*(7), 615–625. https://doi.org/10.1002/we.382

Williams, E., Mushtak, V., Rosenfeld, D., Goodman, S., & Boccippio, D. (2005). Thermodynamic conditions favorable to superlative thunderstorm updraft, mixed phase microphysics and lightning flash rate. *Atmospheric Research*, *76*(1-4), 288–306. https://doi.org/10.1016/j.atmosres.2004.11.009